

Accepted Manuscript

Coupled electronic and morphologic changes in graphene oxide upon electrochemical reduction

Fernando C. Moraes, Renato G. Freitas, Rodrigo Pereira, Luiz F. Gorup, Angel Cuesta, Ernesto C. Pereira

PII: S0008-6223(15)00329-2

DOI: <http://dx.doi.org/10.1016/j.carbon.2015.04.038>

Reference: CARBON 9856

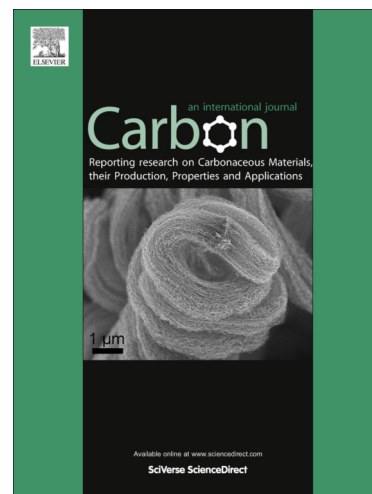
To appear in: *Carbon*

Received Date: 18 February 2015

Accepted Date: 13 April 2015

Please cite this article as: Moraes, F.C., Freitas, R.G., Pereira, R., Gorup, L.F., Cuesta, A., Pereira, E.C., Coupled electronic and morphologic changes in graphene oxide upon electrochemical reduction, *Carbon* (2015), doi: <http://dx.doi.org/10.1016/j.carbon.2015.04.038>

This is a PDF file of an unedited manuscript that has been accepted for publication. As a service to our customers we are providing this early version of the manuscript. The manuscript will undergo copyediting, typesetting, and review of the resulting proof before it is published in its final form. Please note that during the production process errors may be discovered which could affect the content, and all legal disclaimers that apply to the journal pertain.



**Coupled electronic and morphologic changes in graphene oxide upon
electrochemical reduction**

Fernando C. Moraes^a, Renato G. Freitas^{a,b}, Rodrigo Pereira^a, Luiz F. Gorup^a,
Angel Cuesta^c and Ernesto C. Pereira^{a*}

^a Department of Chemistry, Federal University of São Carlos C.P. 676, 13560-970
São Carlos, SP, Brazil

^b Department of Chemistry, Federal University of Mato Grosso, POBox 78060-900,
Cuiaba, MT, Brazil.

^c Department of Chemistry, School of Natural and Computing Sciences, University
of Aberdeen, Aberdeen AB24 3UE, UK

* Corresponding author. Tel.: +55 16 3351 9309. E-mail address: ernesto@ufscar.br
(E.C. Pereira)

Abstract

A systematic study of the electrochemical reduction of graphene oxide was performed. The graphene oxide was reduced electrochemically in phosphate buffer solution by applying potential of -0.8 V for different times. The graphene oxide and the electrochemically reduced graphene oxide were characterized using ex-situ field-emission gun scanning electron microscopy, in-situ Raman scattering and in-situ atomic force microscopy. Raman scattering showed that the reduction process is accompanied by an increase in the ratio between the D and the G bands of graphene, while the microscopies analyses revealed that the reduction procedure promotes changes in the morphology of the graphene oxide sheets that lead to an increase of the system roughness. Electrochemical impedance spectroscopy showed that reduction of graphene oxide promotes a decrease of the charge-transfer resistance upon electrochemical reduction. This observation was in agreement with the changes observed using cyclic voltammetry, which showed a reduction process improve the reversibility and increase the current peak. The increase in the roughness and an improvement of the electronic mobility brought upon electrochemical reduction are a function of the increase in the edge plane-like defects in the graphene layers.

1. Introduction

In the last years, the possibility to develop electrochemical devices based on the use of graphene nanosheets has attracted much attention. Graphene, a single layer of sp^2 carbon atoms with a high electron mobility ($2.0 \times 10^5 \text{ cm}^2 \text{ V}^{-1} \text{ s}^{-1}$) [1] due to its π -conjugated two-dimensional structure, has been the object of intensive research. Graphene has been described as structurally malleable, its electronic, optical and phonon properties making it an interesting material for applications such as solar cells [2], displays [3] and optoelectronic devices [4]. Graphene is also a zero-gap semiconductor. Oxidation of graphene, and the consequent formation of covalent C-O bonds, creates a band gap whose width can be tuned by varying the degree of oxidation. Graphene oxide (GO) is a p -type semiconductor, but it can be converted to an n -type semiconductor by replacing some of the oxygen functionalities by nitrogen-containing groups. This allows GO to be used either as an n - or as a p -type [5] material in photovoltaic systems [6].

From an electrochemical point of view, interesting properties of graphene are its wide potential window (i.e., its electrochemical inertness), its fast charge transfer, and its electrocatalytic activity [7]. These characteristics make of graphene the most widely investigated material for applications in electrochemical devices, such as photoelectrochemical solar cells [8], supercapacitors [9], fuel cells [10], anode for pollutants degradation [11], and electrochemical sensors [12] and biosensors [13].

Graphene can be produced using physical or chemical methods. The most common physical method is graphite exfoliation, including micromechanical [14], sonication [15], microwave [16] and thermal exfoliation [17]. Chemical synthesis includes epitaxial growth using chemical vapor deposition (CVD) over different surfaces [18], as well as the production of exfoliated graphene oxide (GO) in mineral acids using oxidizing agents, as in the Hummers method [19]. However, GO produced by the latter method shows a low conductivity and, consequently, a poor performance as an electrode [20]. This fact is attributed to the existence of a high concentration of oxygenated groups in the basal plane of GO sheets, leading to the formation of electron traps which decrease the charge transfer rate [21]. In order to obtain optimal electrochemical properties, it is necessary to remove these oxygen-containing groups, i.e, to reduce GO to a reduced graphene oxide (RGO) form. RGO can be produced thermally [22], or by

chemical reduction using urea [23], ionic liquid electrolyte [24], sodium borohydrate [25], or hydrazine [26]. An electrochemical reduction procedure has also been proposed, and it has been shown that it results in a more efficient and greener elimination of the unstable oxygenated groups from the GO surface [27], as compared with chemical reduction [28]. When so prepared, the material receives the name of electrochemically reduced graphene oxide (ERGO).

Although electrochemical reduction has been extensively used in the production of ERGO, there are few reports describing a systematic study of the effect of time and potential on the resulting material. In some instances, it has been reported that the removal of oxygenated groups, which leads to an improvement of the electronic properties of GO, is associated to changes in the morphology as a consequence of the reduction process. For example, very recently, den Boer et al. [29] reported a systematic STM study of the reduction of GO, in which it was revealed that the removal of oxygenated functional groups leads to a decrease in the apparent roughness (RMS). Recently, Casero et al. [30] have reported a method to differentiate between GO, RGO, and ERGO, using electrochemical impedance spectroscopy (EIS).

Here we report a systematic study of the changes of the ERGO surface morphology as a consequence of the electrochemical reduction procedure, and correlate those changes with its electrical characteristics. The changes in the apparent roughness of a single GO flake after reduction at the optimal potential and time of -0.8 V and 30 minutes, respectively, were analyzed using *ex-situ* FEG-SEM, *in-situ* Raman scattering, and *in situ* AFM. It was found that an increase of the roughness, as well as of the ratio between the D and G bands of graphene, accompany the changes in the capacitance and charge transfer resistance of ERGO, as measured with EIS and confirmed using cyclic voltammetry (CV).

2. Experimental

2.1 Chemicals and solutions

All chemicals were of analytical grade and were used without further purification. Analytical grade potassium ferricyanide was obtained from Sigma–Aldrich. Phosphate buffer solution (PBS, pH 7.0) of 0.1 mol L⁻¹ ionic strength was used as supporting electrolyte for the fabrication of ERGO, and for the *in-situ* AFM and Raman scattering experiments. The graphene oxide synthesis required graphite powder (< 20 microns),

sodium nitrate, sulfuric acid, nitric acid, potassium permanganate and hydrogen peroxide, all of them purchased from Sigma–Aldrich. All solutions were prepared with pure water from a Millipore Milli-Q system (resistivity > 18.2 MΩ cm).

2.2 Synthesis of graphene oxide

Graphene oxide (GO) was prepared from graphite through a modified Hummers method [19]. A mixture of graphite powder (10.0 g) and sodium nitrate (10.0 g) was attacked with 400.0 mL of 1:3 volume concentrated solution of HNO₃/H₂SO₄ under magnetic stirring in an ice bath. Then, KMnO₄ (50.0 g) was slowly added and the mixture was left reacting under vigorous stirring during 2 hours. Subsequently, the temperature of the mixture was increased to 60 °C and the reaction was allowed to continue at this temperature under stirring for 30 additional minutes, before slowly adding 75 mL of H₂O₂ (30% v/v). Then, 100.0 mL of HCl solution (10% v/v) and 900.0 mL of purified water were added to the mixture, which was kept afterwards in a refrigerator at 4 °C for 24 hours. The light brown supernatant was collected and the graphene oxide was separated by centrifugation at 10000 rpm, and dried by lyophilization during 24 hours.

2.3 Electrode preparation

The working electrodes were prepared by depositing GO on a glassy carbon (GC) substrate (disks 3 mm in diameter for the electrochemical measurements and 10 mm in diameter for the *in-situ* AFM and Raman experiments). Prior to modification, the GC electrode surface was polished with 0.05 μm alumina slurry, rinsed thoroughly with ultrapure water, sonicated 3 minutes in acetone and 3 minutes in water, and dried in air. Meanwhile, 2.0 mg of GO were dispersed in 1.0 mL of ethanol using ultrasonic stirring for 20 min. Aliquots of either 15 μL (3 mm diameter disk) or 50.0 μL (10 mm diameter disks) of this dispersion were placed as a droplet on the GC surface, and the solvent was then allowed to evaporate at room temperature.

2.4 Electrochemical reduction

The electrochemical reduction of GO was performed potentiostatically. The freshly prepared GC electrode modified with the GO film was polarized at -0.8 V vs. Ag/AgCl (3 M KCl) for different times. The resulting ERGO was characterized after these reduction steps. For electrochemical characterization, the electrode was removed from the cell, rinsed with Milli-Q water and inserted in a different electrochemical cell

containing the redox couple. In the case of the *in-situ* AFM and Raman experiments, the reduction and the characterization steps were performed in the same cell and using the same solution (phosphate buffer, pH7).

2.5 Apparatus and procedure

CV experiments were performed using an Autolab potentiostat, Model PGSTAT302 (Eco Chemie, Utrecht, Netherlands), coupled to a personal computer and controlled with NOVA software. A GC disk modified with a GO film was used as the working electrode, a Ag/AgCl (3 M KCl) electrode, to which all the potentials in the text are referred, was used as reference, and a Pt plate was used as the auxiliary electrode. Cyclic voltammograms were registered in 0.1 M H₂SO₄ + 1.0 mM K₃[Fe(CN)₆] solutions in a potential range from -0.2 to +0.8 V with a scan rate of 50 mV s⁻¹. All experiments were carried out at a controlled temperature of 25 ± 1 °C.

EIS data were obtained using a PC-controlled FRA2 (Eco Chemie, Utrecht, Netherlands) frequency response analyzer coupled to an Autolab potentiostat (model PGSTAT302, Eco Chemie, Utrecht, Netherlands). The frequency of the AC wave was scanned between 10 kHz and 10 mHz (10 data points per frequency decade), with a 10 mV amplitude. The measurements were carried out in 0.1 M H₂SO₄ + 1.0 mM K₃[Fe(CN)₆] solutions. The impedance spectra were analyzed using the EQUIVCRT software, and the Randles equivalent circuit was used to fit the experimental results and determine the electrical parameter values for each experiment.

In situ EC-AFM images were obtained using an Agilent AFM series 5500 (Agilent Technologies). Imaging was carried out in the acoustic AC mode (AAC mode) using a silicon cantilever and Si tip (NanoSensors, Neuchatel, Switzerland) with a typical spring constant of C= 21 N/m and a typical resonance frequency between 146 and -236 kHz. The *in situ* AFM studies were carried out in an electrochemical cell in which the AFM scanner was inserted from above. The AFM liquid cell (Supplementary information S1) was made from Kelf-F and has a circular hole 20 mm in diameter at its center, in which the disk-shaped sample surface is kept in place with the help two screws and retaining clips. A viton O-ring was used to avoid leaks. The measurements were carried out with a three-electrode setup. The working electrode was the disk placed at the bottom of the cell, and the reference electrode was a silver wire 0.25 mm in diameter immersed in the electrolyte. The counter electrode was a Pt wire 0.25 mm in diameter. The electrode potential was controlled using an Autolab potentiostat (model PGSTAT302, Eco

Chemie, Utrecht, Netherlands) coupled to a personal computer and controlled with NOVA software.

In situ Raman spectra were performed using the same electrochemical cell described above and used in the AFM experiments. The spectra were collected after different times of GO electrochemical reduction, using a fixed sample support in order to be sure that a single point of the graphene was analyzed. A Horiba/Join Yvon Labran dispersive Raman spectrometer equipped with an Olympus BX41 microscope was used. The measurements were performed with excitation at 540 nm and using a 10x magnification lens. The spectra were collected at Raman shifts between 1100 and 1850 cm^{-1} with 10 second and 10 cycles of exposure.

The *ex-situ* microscopies of the GO and ERGO were examined using Field-Emission Gun Scanning Electron Microscopy (FEG-SEM) recorded with a FEG-Zeiss model Supra 35 VP (Zeiss, Germany). The high-resolution transmission electron microscope images were recorded using a ZEISS EM912 Omega e STEM, Germany).

3. Results and discussion

Comparison of *ex-situ* FEG-SEM images of a GO sample recorded before (Fig. 1A) and after (Fig. 1B) the reduction process at -0.8 V in phosphate buffer solution (PBS, pH 7.0) during 30 min reveals a severe change in the morphology of GO. In the high-resolution TEM image of the GO (Fig. 1C) it was observed that the GO surface was completely flat. However, in the TEM images of the ERGO (Fig. 1D), it was clear to observe the presence of dark regions with high contrast, showing that the surface became roughness. Electrochemical reduction induces a considerable roughening, wrinkling and folding of GO. The purpose of the following characterization is to understand the nature and consequences of these changes.

Raman scattering has been successfully applied to carbon materials as an efficient characterization method, including the identification of single layer features and edge orientation in graphene, strain evaluation, determination of doping concentration, as well as probing of electron-phonon interactions [31,32]. In the present case, we used Raman spectroscopy focused on a specific area of the sample, which allowed us to monitor the amount of disorder caused by the electrochemical reduction. The use of Raman microscopy is necessary because different areas of a graphene sample with different defect densities or different types of defects could show different G-peak

frequencies and FWHM, as well as different I_D/I_G ratios, as observed by Cançado et al. [33]. Fig. 2A shows a sequence of in-situ Raman spectra collected from a $100 \mu\text{m}^2$ area during the electrochemical reduction of graphene oxide at -0.8 V . The typical G and D bands at ca. 1580 and 1350 cm^{-1} , respectively, are clearly observed. As expected, initially the G-band is more intense than the D-band, since the former, related to E_{2g} optical phonons of the plane bond-tangential stretching motion of pairs of sp^2 C-atoms [34], is the primary mode in graphene [35], while the latter corresponds to the breathing mode of 6 sp^2 carbon rings, and requires defects (bond-angle disorder, bond-length disorder, or an heteroatom-induced change in hybridization) to be activated. The D band is typically very weak in graphite and graphene because of their crystal symmetries [36].

The large intensity of the D-band in the spectra in Fig. 2A indicates that there are many defects in the material. Furthermore, upon electrochemical reduction the intensity of the D-band increases considerably, while that of the G-band decreases, but only slightly. This provokes an inversion of the relative band intensity, which was observed to be a function of reduction time, as clearly shown in the I_D/I_G vs. time plot presented in Fig. 2B. The I_D/I_G ratio continually increases with increasing reduction time at -0.8 V from an initial value of 0.67 . The increase is approximately linear at short times, and levels off to 1.5 after 30 min of reduction, remaining roughly constant at longer reduction times. As described in the literature [37], the I_D/I_G ratio is related to an increase in the disorder present in the material. In GO, sp^3 carbon atoms occur bonded to oxygen-containing functional groups, such as hydroxyl, carboxyl and epoxide. As reduction proceeds, these bonds are broken and the oxygenated species is most likely removed from the surface. In GO form, the number of basal-plane graphitic regions is higher than the edge-plane ones. The increase in the I_D/I_G ratio could be related to different kinds of lattice defects whose concentration increases as the reduction proceeds [38]. The increase in the I_D/I_G ratio suggests that the main effect caused by electrochemical reduction is an increase in the number edge plane-like defects in the graphene sheet. These lattice defects are expected to have a direct influence in the electron mobility of the sample, because the resulting ribbons act as optical waveguides or quantum dots, allowing electrons to flow smoothly along the ribbon edges [39]. Hallam et al. [40] have shown that the electron transfer rate of the edge plane is faster than that of the basal plane. Consequently, interfacial electron transfer will be more effective in the presence

of a large amount of edge plane-like defects, and this quantity will dictate the overall electrochemical properties of ERGO [41].

The electrochemical effect of the reduction process on the GO sample was evaluated using electrochemical impedance spectroscopy (EIS). We chose to use the $[\text{Fe}(\text{CN})_6]^{4-/3-}$ redox couple in solution, for which the charge transfer resistance can be determined quantitatively, thus making the interpretation of the experimental data easier than when evaluating only interfacial capacitance in the absence of a redox couple. The spectra were collected at +0.25 V, which coincided with the open circuit potential (OCP) of the GO electrode before reduction, after each reduction step at -0.8 V. Fig. 3A presents the obtained results. As observed in Fig. 3A, the Nyquist diagram consists of a semicircle at higher frequencies, followed by a straight line with slope close to 45° at lower frequencies, indicating a redox process under mixed kinetic and diffusional control, as expected in the present case at the potential employed. A decrease in the diameter of the semicircle diameter with increasing reduction time is clearly observed, which is related to a decrease in the charge-transfer resistance, R_{ct} . We have used an Ershler-Randles equivalent circuit with a Warburg element in series (Fig. 3A-inset), which has been proposed in the literature to describe the electrochemical behavior of graphene [42,43], although we found it necessary to replace the ideal double layer capacitance by a constant phase element CPE_{dl} , whose impedance is:

$$Z_{CPE} = T^{-1}(i\omega)^{-\alpha} \quad \text{Eq. 1}$$

with $i = \sqrt{-1}$, $\omega = 2\pi f$, and T a frequency-independent proportionality constant whose physical meaning is determined by the value of the exponential factor, α [44]. The exponent parameter α is usually smaller than 1, and the mean capacity of the double layer may be estimated according to the Brug formula [45]:

$$C_{dl} = T^{1/\alpha} \left(\frac{1}{R_s} + \frac{1}{R_{ct}} \right)^{1-1/\alpha} \quad \text{Eq. 2}$$

Where R_s and R_{ct} are the solution resistance and the resistance of charge transfer, respectively.

The values of R_{ct} , C_{dl} and α that result from fitting the experimental EIS data to the equivalent circuit are shown in Fig. 3B, and reflect the effect of the reduction time on the structural and electronic properties of ERGO. It is evident from Figure 3B that the R_{ct} of

ERGO is reduced to 29 % of the original value for GO after 30 min of reduction at -0.8 V.

Previous studies have reported that GO is an insulating material due to its disrupted sp^2 structure [46,47], which leads to a severe decrease in the charge carrier mobility. The decrease in R_{ct} associated to the reduction of GO observed herein can be related to the increase in the conductivity of ERGO due to the removal of oxygen and the partial restoration of graphene's sp^2 structure, as has been observed using XPS [48,49]. A similar behavior was reported by Casero et al. [30], who performed EIS experiments with the aim of comparing the photocatalytical and the electrochemical methods of obtaining reduced graphene. These authors observed Nyquist diagrams with profiles similar to those reported here, and reported lower R_{ct} values for ERGO than for photocatalytically reduced GO. They observed an approximately 3.5 times smaller R_{ct} for ERGO than for GO, with photocatalytically reduced GO showing intermediate values closer to that of GO, which were attributed to an incomplete reduction.

CV in 0.1 mol L⁻¹ of H₂SO₄ containing 1.0 mmol L⁻¹ of K₃[Fe(CN)₆] was also used to characterize GO and ERGO (the latter, produced after electrochemical reduction of GO in PBS at -0.8 V during 30 minutes). As shown in Fig. 4, the oxidation peak occurs on ERGO at a potential 0.095 V more negative than on GO, which decreases the separation between the reduction and oxidation peaks, ΔE_p , of the [Fe(CN)₆]^{3-/4-} redox couple from 185 mV on GO to 65 mV on ERGO. This result is consistent with the decrease in R_{ct} observed using EIS. A 2-fold increase in the peak current on ERGO as compared to GO electrode is also observed. The electrochemical areas of these two electrodes were evaluated by comparing the respective peak current values following the Randles-Sevcik equation [50]. This yielded an electroactive area of 0.070 cm² for the GO electrode and of 0,209 cm² for the ERGO electrode after 30 minutes of reduction at -0.8 V, in qualitative agreement with previous studies.

Fig. 5 shows AFM images of a single GO flake recorded after different reduction times at -0.8 V. It can be clearly observed in Fig. 5 that the reduction process provokes the flake to wrinkle and fold (see, *e.g.*, the areas marked with arrows in Fig. 5), in good agreement with the *ex-situ* FEG-SEM results reported in Fig. 1.

Based on this information, we chose a region in which the modification of the surface morphology appeared particularly severe, and performed a deeper study of the changes in the topography and roughness experienced by the flake upon reduction. The results are illustrated in Fig. 6. Fig. 6A shows topographic images of this region, as well as

topographic line profiles, of pristine GO, and of ERGO produced after 30 and 60 min of reduction at $E = -0.8$ V (GO, ERGO-30 and ERGO-60, respectively). Line profile 1 falls completely within the graphene flake, while line profile 2 goes from the surface of the GC substrate into the surface of the flake. In both cases, the profiles show a clear change in the flake's roughness after the electrochemical reduction step. In particular, the height difference between the lower and higher lying areas of the flake has increased by about 50%, when the profiles for GO and those for ERGO after 60 minutes of reduction are compared.

We also determined the apparent RMS roughness (R_q) of the pristine GO and of ERGO produced after reduction steps of different duration (Fig. 6B). A typical value of the R_q for GO of 0.26 nm was found. R_q increases sharply with increasing time at short reduction times, but levels off at a roughly constant value of 0.72 nm after 30 minutes of reduction. Comparison with EIS measurements allows us to provide a link between the structural and electronic changes observed upon formation of ERGO. Interestingly, a linear plot is obtained when R_q is plotted versus α values, as obtained from the EIS experiments described above (Fig. 6C). The non-ideality (i.e., a value of $\alpha < 1$) in the behavior of C_{dl} , as obtained from the impedance spectra, can be related with high values of the surface roughness factor [44]. In the present case, the ERGO surface is composed by small cracked flakes, which lead to high roughness values. Bidoia et al. [51] have proposed a direct correlation between the value of α and the surface roughness, a correlation which is clearly observed in Fig. 6C. This is, in our opinion, the first solid evidence that both the wrinkling of the graphene flakes and the higher electrochemical activity of ERGO, as compared with GO, have a common origin, namely, the creation during the reduction process of edge plane-like defects in the graphene sheet, as evidenced by Raman scattering (see above).

The clear increase of the surface roughness of ERGO with increasing reduction time reported here is in contradiction with the recent report by dem Boer et al. [29], in which the local deoxygenation of GO via chemical reduction was reported to induce a decrease in the apparent roughness. However, we must emphasize that our AFM and Raman data (which indicate that electrochemical reduction leads to an increase of the number of defects and results in a pseudo strain component) are consistent with each other in suggesting that the GO surface becomes less planar after electrochemical reduction. The almost 3-fold increase of the R_q after the electrochemical reduction step is consistent with a previous report by Bagri et al. [52], according to which the deoxygenation of GO

causes a strain on the C-O bond, and the removal of the functional groups results in the rupture of the C-O bond, forming holes, defects, as well as five and seven member rings, within the graphene structure. The so generated strain provokes the graphene surface to bend and wrinkle.

4. Conclusions

In conclusion, electrochemical reduction provoked a clear wrinkling and folding of the GO surface, as revealed using *ex-situ* FEG-SEM and *in-situ* AFM. These topographical modifications occurred concomitantly with important changes in the electronic and electrochemical properties of ERGO, as revealed by EIS and CV, which were shown to be due to an increase in the electronic mobility and in the electrochemically active surface area. *In-situ* Raman scattering revealed that these changes are associated to an increase in the I_D/I_G ratio, which we have attributed to an increase in the number of edge plane-like defects in the graphene sheets due to the rupture of bonds between carbon atoms and oxygen-containing functionalities, and the subsequent removal of oxygenated species from the surface, during the reduction process. The creation of these defects must be the common origin of the observed topographical modifications and increased electronic mobility.

Acknowledgements

AC gratefully acknowledges to CAPES (Proj. N° A090/2013), FAPESP (Proj. N°. 2013/07296-2) and CNPq for financial support.

References

- [1] Geim A.K. Graphene: status and prospects. *Science* 2009;324:1530-1534.
- [2] Roy-Mayhew J.D, Bozym D.J, Punckt C, Aksay I. Functionalized graphene as a catalytic counter electrode in dye-sensitized solar cells, *ACS Nano* 2010;4:6203–6211.
- [3] Novoselov K.S, Fal'ko VI, Colombo L, Gellert PR, Schwab MG, Kim K. A roadmap for graphene, *Nature* 2012;490:192–200.
- [4] Bao Q, Loh KP. Graphene photonics, plasmonics, and broadband optoelectronic devices, *ACS Nano* 2012;6:3677–3694.
- [5] Fuhrer MS, Lau CN, MacDonald AH. Graphene: materially better carbon, *MRS Bull.* 2010;35:289-295.
- [6] Yeh T, Cihlár J, Chang CY, Cheng C, Teng H. Roles of graphene oxide in photocatalytic water splitting. *Mater. Today* 2013;16:78 – 84.
- [7] Zeng F, Sun Z, Sang X, Diamond D, Lau KT, Liu X, Su DS. In situ one-step electrochemical preparation of graphene oxide nanosheet-modified electrodes for biosensors, *ChemSusChem* 2011;4:1587 – 1591.
- [8] Zhang W, Bai HC, Zhang Y, Sun Y, Lin S, Liu J, Yang Q, Song XM. Enhanced photovoltaic effect of ruthenium complex-modified graphene oxide with p-type conductivity, *Mater. Chem. Phys.* 2014;147:1140-1145.
- [9] Yang J, Gunasekaran S. Electrochemically reduced graphene oxide sheets for use in high performance supercapacitors, *Carbon* 2013;51:36–44.
- [10] Paneri A, Heo Y, Ehlert G, Cottrill A, Sodano H, Pintauro P, Moghaddam S. Proton selective ionic graphene-based membrane for high concentration direct methanol fuel cells, *J. Membrane Sci.* 2104;467:217-225.
- [11] Vadivel S, Kamalakannan VP, Keerthi B, Balasubramanian N. D-Pencillamine assisted microwave synthesis of Bi₂S₃ microflowers/RGO composites for photocatalytic degradation-A facile green approach, *Ceram. Int.* 2014;40:14051-14060.
- [12] Cincotto FH, Moraes FC, Machado SAS. Graphene nanosheets and quantum dots: a smart material for electrochemical applications, *Chem. Eur. J.* 2014;20:4746 – 4753.

- [13] Barsan MM, Prathish KP, Sun XL, Brett CMA. Nitrogen doped graphene and its derivatives as sensors and efficient direct electron transfer platform for enzyme biosensors, *Sens. Actuators, B* 2014;203:579-587.
- [14] Jang BZ, Zhamu A. Processing of nanographene platelets (NGPs) and NGP nanocomposites, a review. *J. Mater. Sci.* 2008;43:5092–5101.
- [15] Blake P, Brimicombe PD, Nair RR, Booth TJ, Jiang D, Schedin F, Ponomarenko LA, Morozov S, Gleeson HF, Hill EW, Gein AK, Novoselov KS. Graphene-based liquid crystal device. *Nano Lett.* 2008;8:1704-1708.
- [16] Zhu Y, Murali S; Stoller MD, Velamakanni A, Piner RD, Rouff RS. Microwave assisted exfoliation and reduction of graphite oxide for ultracapacitors, *Carbon* 2010;48:2106 – 2122.
- [17] McAllister MJ, Li JL, Adamson DH, Schniepp HC, Abdala AA, Jun L, Herrera-Alonso M, Milius DL, Car R, Prud'homme R.K, Aksay A. Single sheet functionalized graphene by oxidation and thermal expansion of graphite. *Chem. Mater.* 2007;19:4396–404.
- [18] Berger C, Song ZM, Li XB, Wu XS, Brown N, Naud C, Mayou D, Hass J, Marchenkov AN, Conrad EH, First PN, de Heer WA. Electronic confinement and coherence in patterned epitaxial graphene. *Science* 2006;312:1191–1196.
- [19] Hummers WS, Offeman RE. Preparation of Graphitic Oxide, *J. Am. Chem. Soc.* 1958;80:1339.
- [20] Li ZJ, Yang BC, Zhang SR, Zhao CM. Graphene oxide with improved electrical conductivity for supercapacitor electrodes. *App. Surf. Sci.* 2012;258:3726 – 3731.
- [21] Liu H, Zhang L, Guo Y, Cheng C, Yang L, Jiang L, Yu G, Hu W, Liu Y, Zhu D. Reduction of graphene oxide to highly conductive graphene by Lawesson's reagent and its electrical applications. *J. Mater. Chem. C* 2013;1:3104–3109.
- [22] Sun A, Zheng J, Sheng Q, A highly sensitive non-enzymatic glucose sensor based on nickel and multi-walled carbon nanotubes nanohybrid films fabricated by one-step coelectrodeposition in ionic liquids. *Electrochim. Acta* 2012;65:64–69.
- [23] Lei ZB, Lu L, Zhao XS, The electrocapacitive properties of graphene oxide reduced by urea. *Energy Environ. Sci.* 2012;5:6391–6399.
- [24] Chen Y, Zhang X, Zhang D, Yu P, Ma Y. High performance supercapacitors based on reduced graphene oxide in aqueous and ionic liquid electrolytes. *Carbon* 2011;49:573–580.

- [25] Shin HJ, Kim KK, Benayad A, Yoon SM, Park HK, Jung IS, Jin MH, Jeong HK, Kim JM, Choi JY, Lee YH. Efficient reduction of graphite oxide by sodium borohydride and its effect on electrical conductance. *Adv. Funct. Mater.* 2009;19:1987–1992.
- [26] Park S, An J, Potts JR, Velamakanni A, Murali S, Ruoff RS, Hydrazine-reduction of graphite- and graphene oxide. *Carbon* 2011;49:3019 – 3023.
- [27] Guo HL, Wang XF, Qian QY, Wang FB, Xia XH. A green approach to the synthesis of graphene nanosheets. *ACS Nano* 2009;3:2653–2659.
- [28] Peng XY, Liu XX, Diamond D, Lau KT. Synthesis of electrochemically-reduced graphene oxide film with controllable size and thickness and its use in supercapacitor. *Carbon* 2011;49:3488–3496.
- [29] den Boer D, Weis JG, Zuniga CA, Sydlik SA, Swager TM. Apparent roughness as indicator of (local) deoxygenation of graphene oxide. *Chem. Mater.* 2014;26:4849-4855.
- [30] Casero E, Parra-Alfambra AM, Petit-Dominguez MD, Pariente F, Lorenzo E, Alonso C. Differentiation between graphene oxide and reduced graphene by electrochemical impedance spectroscopy (EIS), *Electrochem. Commun.* 2012;20:63-66.
- [31] Cong C, Yu T, Wang H. Raman study on the g mode of graphene for determination of edge orientation. *ACS Nano* 2010;4:3175-3180.
- [32] Ferrari C, Robertson J. Interpretation of Raman spectra of disordered and amorphous carbon. *Phys. Rev. B* 2000;61:14095-14107.
- [33] Cañado LG, Jorio A, Ferreira EHM, Stavale F, Achete CA, Capaz RB, Moutinho MVO, Lombardo A, Kumala TS, Ferrari AC. Quantifying defects in graphene via Raman spectroscopy at different excitation energies. *Nano Lett.* 2011;11:3190-3196.
- [34] Kaniyoor A, Ramaprabhua SA. Raman spectroscopic investigation of graphite oxide derived graphene. *AIP Adv.* 2012;2(032183):1-13.
- [35] Sato K, Saito R, Oyama Y, Jiang J, Cañado LG, Pimenta MA, Jorio A, Samsonidze GG, Dresselhaus G, Dresselhaus MS. D-band Raman intensity of graphitic materials as a function of laser energy and crystallite size. *Chem. Phys. Lett.* 2006;427:117-121.

- [36] Tuinstra F, Koenig JL. Raman Spectrum of Graphite. *J. Chem. Phys.* 1970;53:1126-1130.
- [37] Tai FC, Lee SC, Wei CH, Tyan SL. Correlation between I_D/I_G ratio from visible Raman spectra and sp^2/sp^3 ratio from XPS spectra of annealed hydrogenated DLC film. *Mater. Trans.* 2006;47:1847-1852.
- [38] Chen JH, Cullen W, Jang C, Fuhrer M, Williams E. Defect scattering in graphene. *Phys. Rev. Lett.* 2009;102:236805.
- [39] Baringhaus J, Ruan M, Edler F, Tejada A, Sicot M, Taleb-Ibrahimi A, Li AP, Jiang Z, Conrad EH, Berger C, Tegenkamp C, De Heer WA. Exceptional ballistic transport in epitaxial graphene nanoribbons. *Nature* 2014;506:349-354.
- [40] Hallam PM, Banks CE. Quantifying the electron transfer sites of graphene. *Electrochem. Commun.* 2011;13:8-11.
- [41] Kampouris DK, Banks CE. Exploring the physicoelectrochemical properties of graphene. *Chem. Commun.* 2010;46:8986-8988.
- [42] Molina J, Fernandez J, del Rio AI, Bonastre J, Cases F. Chemical and electrochemical study of fabrics coated with reduced graphene oxide. *App. Surf. Sci.* 2013;279:46-54
- [43] Zhang D, Zhang Y, Zheng L, Zhang Y, He L. Graphene oxide/poly-l-lysine assembled layer for adhesion and electrochemical impedance detection of leukemia K562 cancer cells. *Biosens. Bioelectron.* 2013;42:112-118.
- [44] Pajkossy T. Impedance spectroscopy at interfaces of metals and aqueous solutions – Surface roughness, CPE and related issues. *Solid State Ionics* 2005;176:1997-2003.
- [45] Bandarenka AS. Exploring the interfaces between metal electrodes and aqueous electrolytes with electrochemical impedance spectroscopy. *Analyst* 2013;138:5540-5554.
- [46] Loh KP, Bao Q, Ang PK, Yang J. The chemistry of graphene. *J. Mater. Chem.* 2010;20:2277-2289.
- [47] Liu H, Liu Y, Zhu D. Chemical doping graphene *J. Mater. Chem.* 2011;21:3335-3345.
- [48] Dreyer DR, Park S, Bielawski CW, Ruoff RS. The chemistry of graphene oxide. *Chem. Soc. Rev.* 2010;39:228-240.
- [49] Chen D, Feng H, Li JJ. Graphene oxide: preparation, functionalization, and electrochemical applications. *Chem. Rev.* 2012;112:6027-6053.

- [50] Bard AJ, Faulkner LR. *Electrochemical Methods: Fundamental and Applications*, Wiley Interscience, 2001.
- [51] Bidoia E.D, Bulhoes L.O.S, Rocha-Filho R.C. Pt/HClO₄ interface CPE: Influence of surface roughness and electrolyte concentration. *Electrochim. Acta* 1994;39:763-769.
52. Bagri, A.; Mattevi, C. Acik, M.; Chabal, Y. J.; Chhowalla, M.; Shenoy, V. B. Structural evolution during the reduction of chemically derived graphene oxide. *Nat. Chem.* **2010**, 2, 581-587.

ACCEPTED MANUSCRIPT

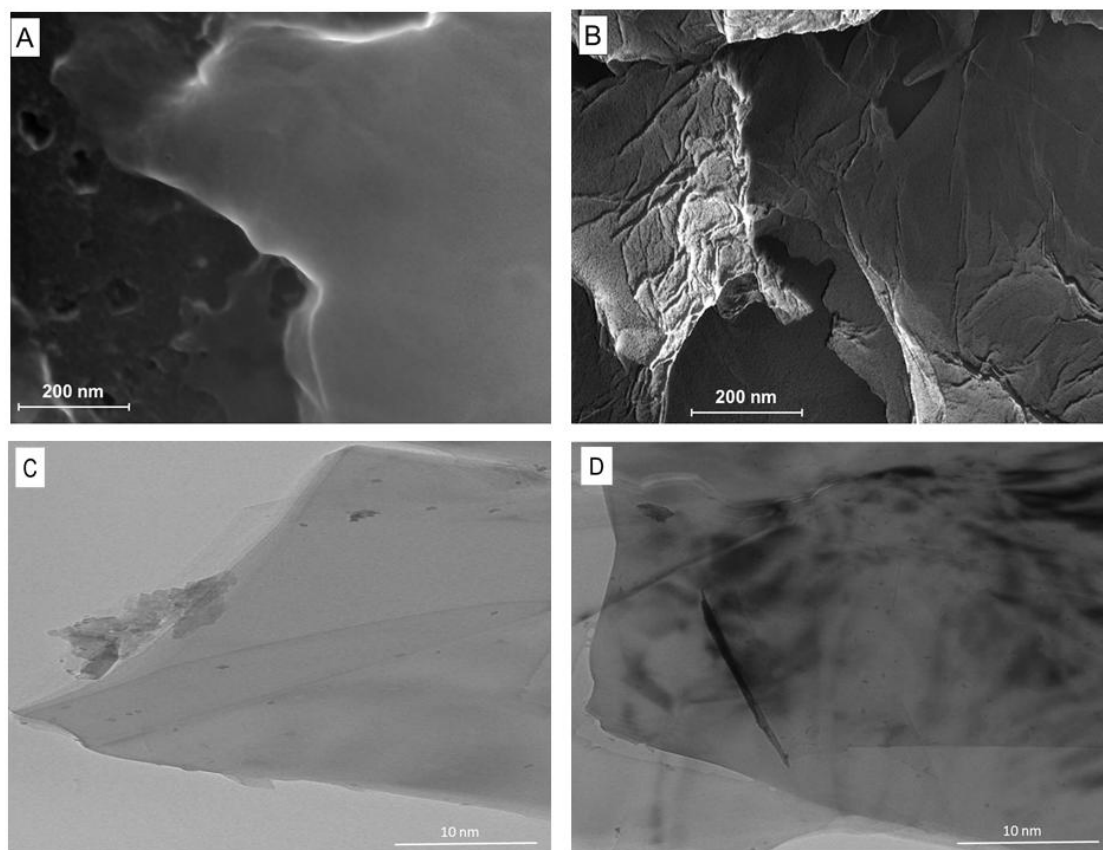


Fig. 1. *Ex-situ* FEG-SEM images of pristine GO (A) and of ERGO (B) after 30 min of potentiostatic reduction in phosphate buffer solution (pH 7) at -0.8 V vs. Ag/AgCl (KCl_{sat}). *Ex-situ* TEM images of pristine GO (C) and of ERGO (D) with the same conditions described above.

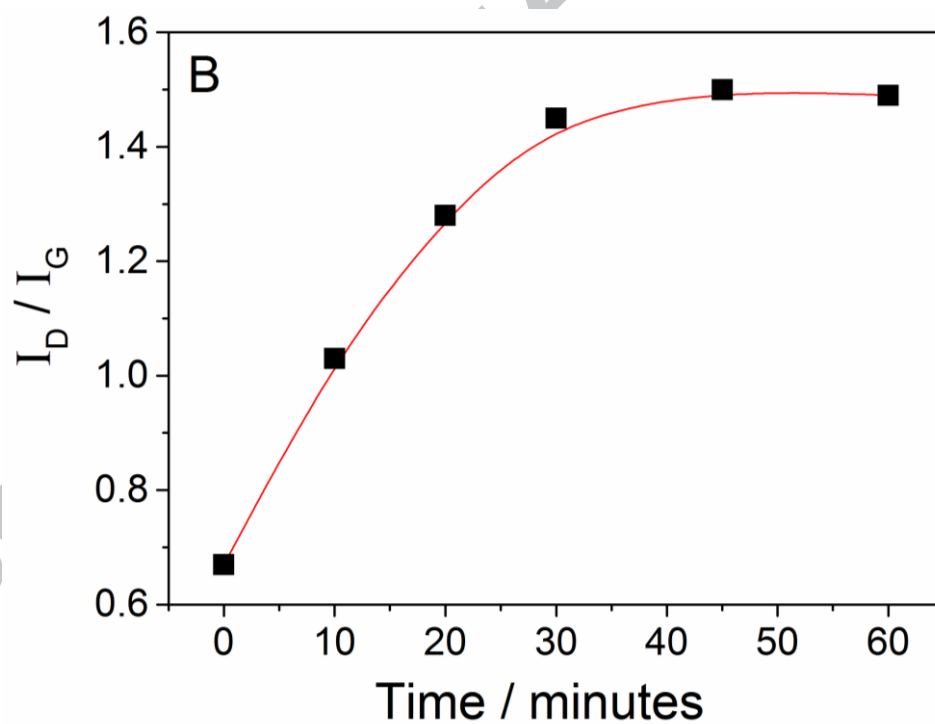
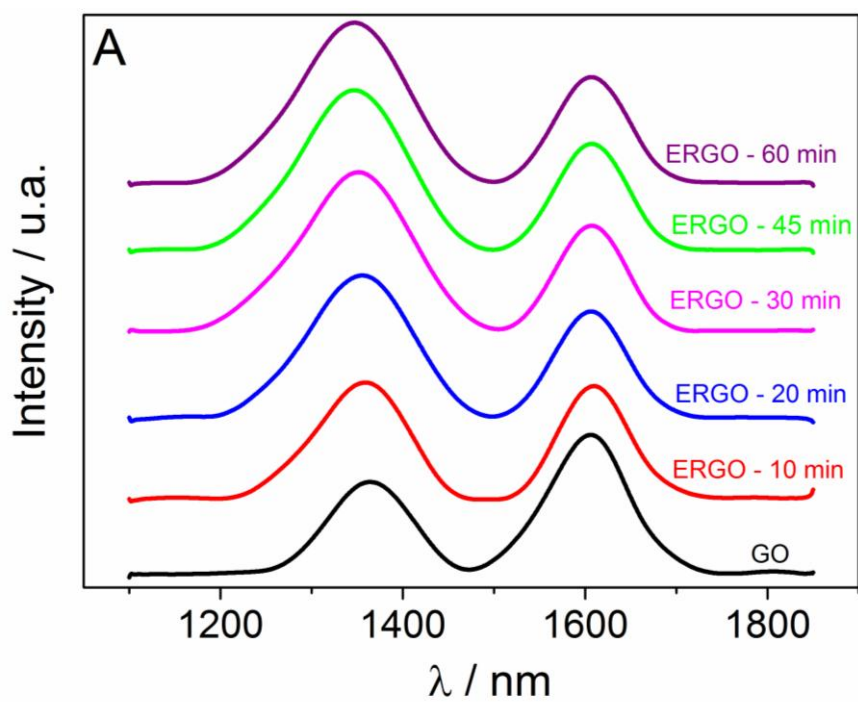


Fig. 2. (A) *In-situ* Raman spectra in phosphate buffer solution (pH 7) of GO (black line) and of ERGO after 10 (red line), 20 (blue line), 30 (pink line), 45 (green line), and 60 (violet line) min of potentiostatic reduction at -0.8 V vs. Ag/AgCl (KCl_{sat}) in the same solution. (B) I_D/I_G ratio as a function of reduction time.

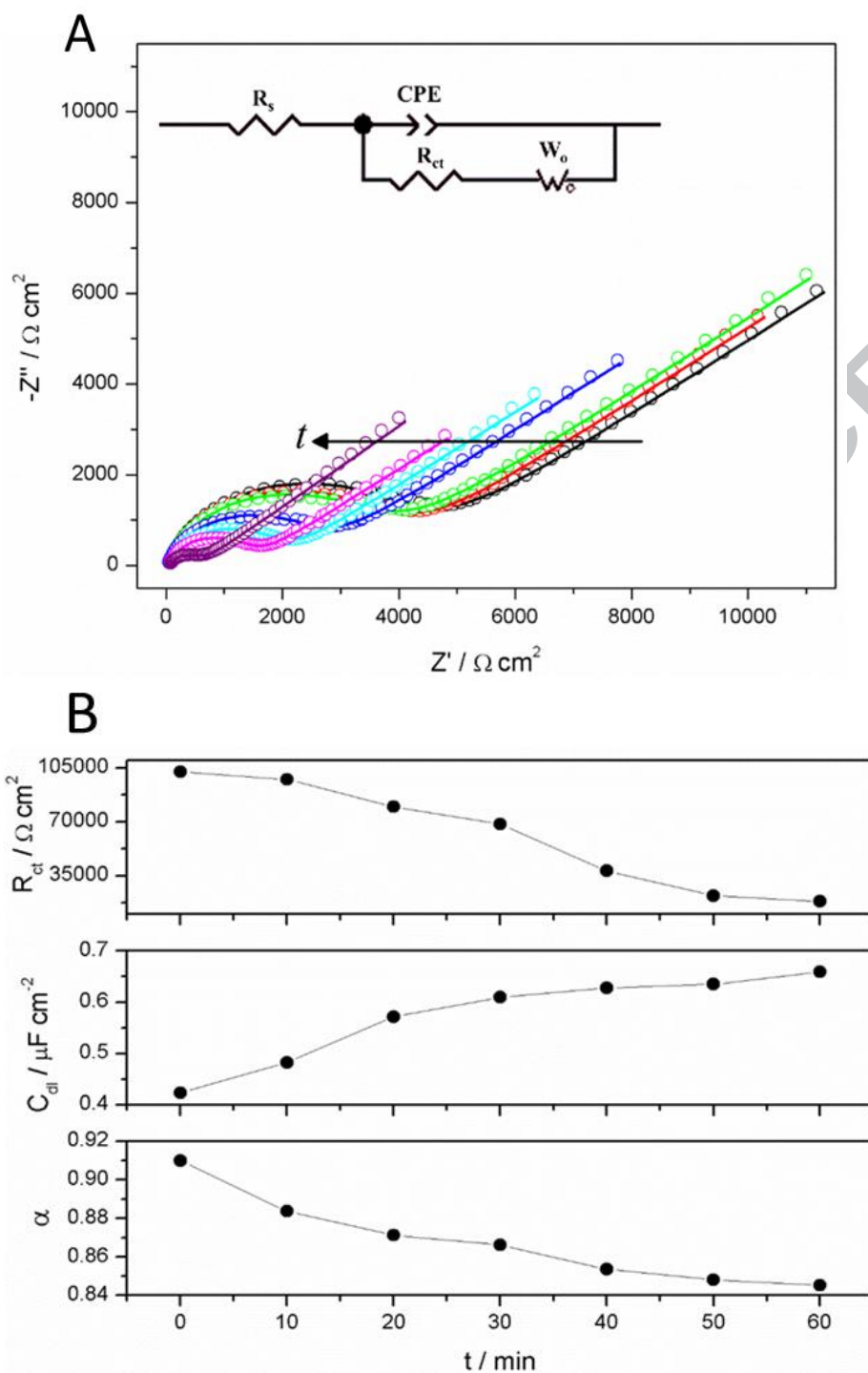


Fig. 3. (A) Nyquist diagrams in 0.1 M H_2SO_4 + 1.0 mM $\text{K}_3[\text{Fe}(\text{CN})_6]$ of GO (black line), and of ERGO after 10 (red line), 20 (blue line), 30 (pink line), 45 (green line), and 60 (violet line) min of potentiostatic reduction in phosphate buffer solution (pH 7) at -0.8 V vs. Ag/AgCl (KCl_{sat}). Inset: equivalent electrical circuit. (B) Electrochemical impedance parameters obtained from fitting the data in Figure 3A to the equivalent electrical circuit in the corresponding inset.

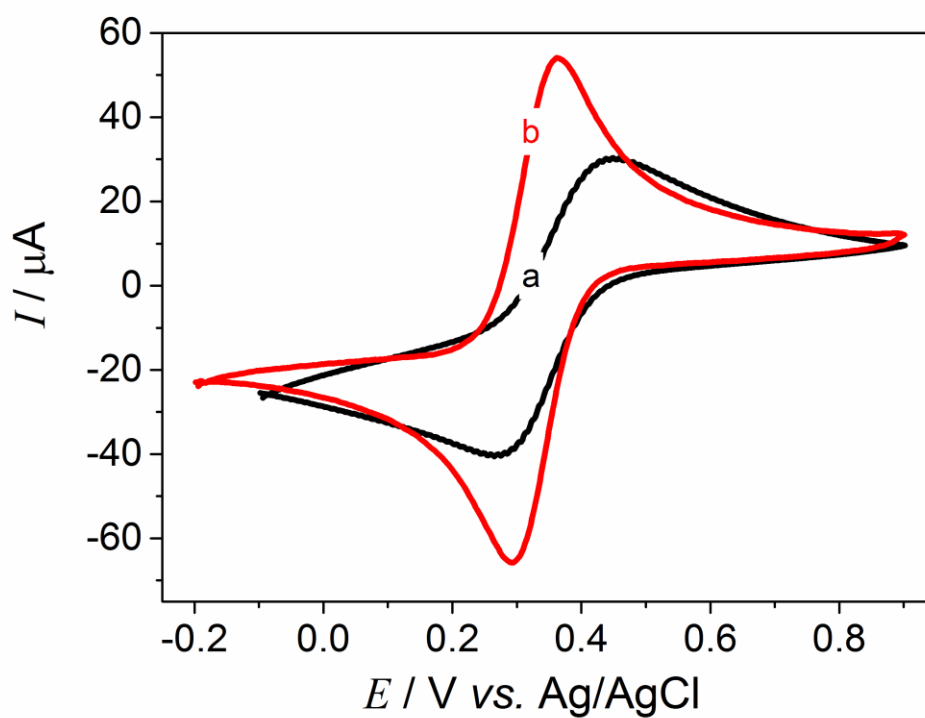


Fig. 4. Cyclic voltammograms in 0.1 M H_2SO_4 + 1.0 mM $\text{K}_3[\text{Fe}(\text{CN})_6]$ of (a) pristine GO and (b) ERGO after 30 min of potentiostatic reduction in phosphate buffer solution (pH 7.0) at -0.8 V vs. Ag/AgCl (KCl_{sat}).

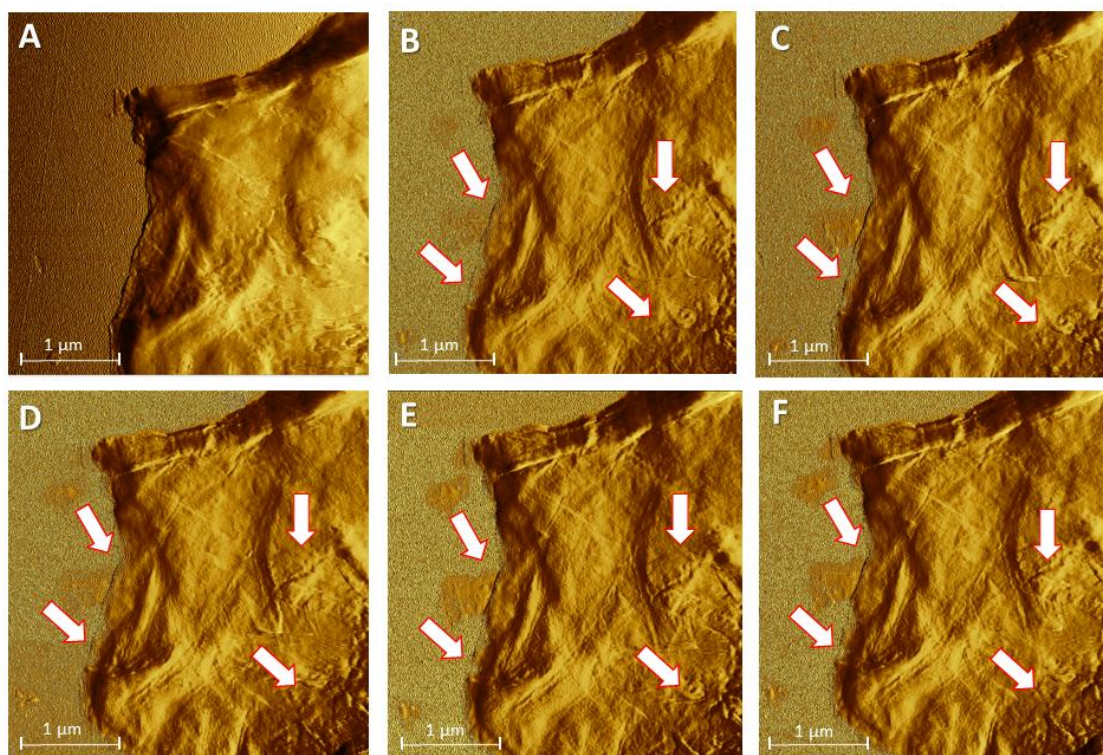


Fig. 5. *In-situ* AFM images in phosphate buffer solution (pH 7) of pristine GO (A) and of ERGO after 10 (B), 20 (C), 30 (D), 45 (E), and 60 (F) min of potentiostatic reduction at -0.8 V vs. Ag/AgCl (KCl_{sat}) in the same solution.

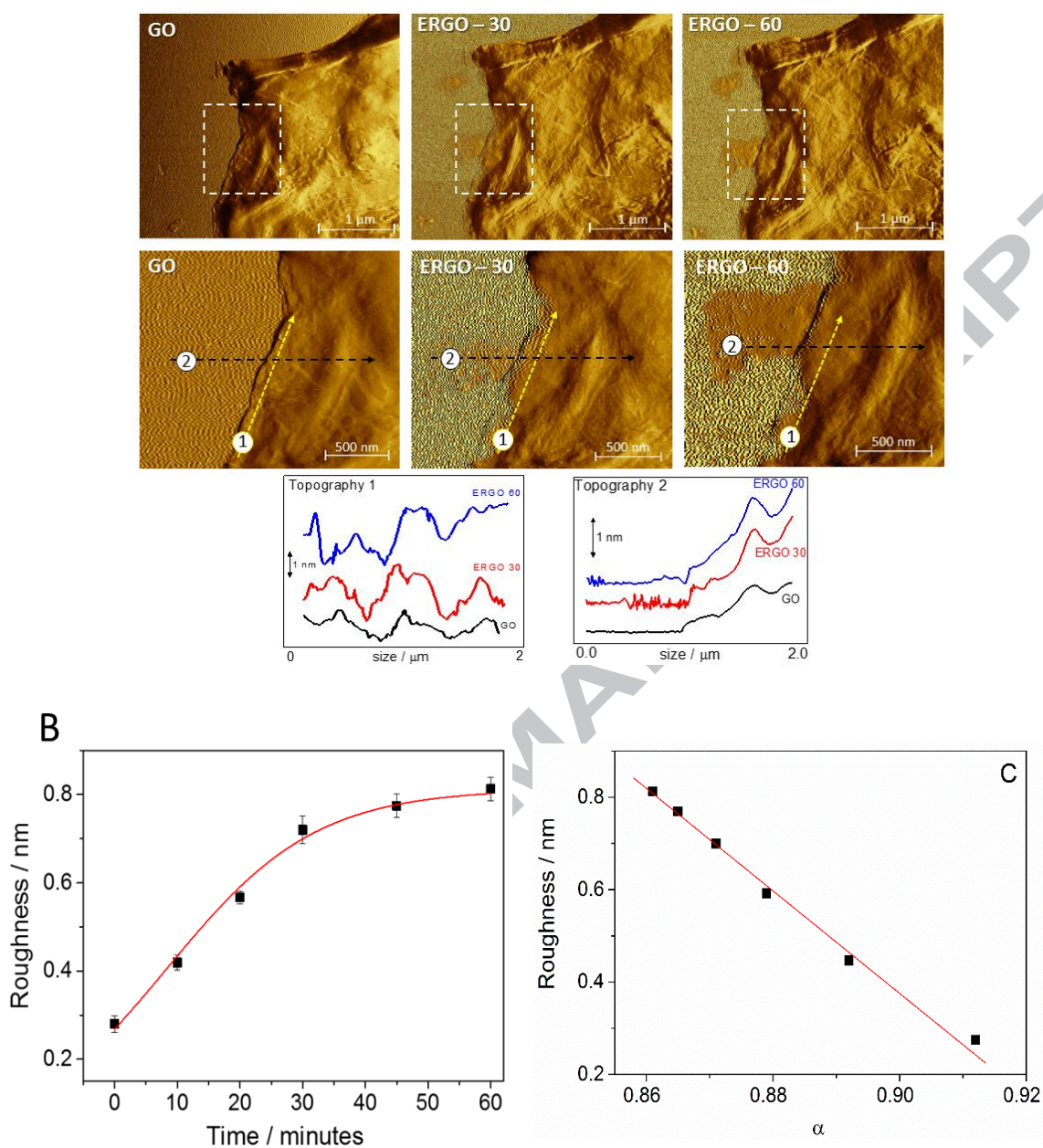


Fig. 6. (A) *In-situ* AFM images in phosphate buffer solution (pH 7) of pristine GO, and of ERGO after 30 (ERGO-30) and 60 (ERGO-60) min of potentiostatic reduction at -0.8 V vs. Ag/AgCl (KCl_{sat}) in the same solution. The images in the bottom row correspond to a zoom into the areas within the squares in the top-row images. The figures labelled Topography 1 and Topography 2 correspond to topographic profiles across lines 1 and 2, respectively, in the bottom-row images. (B) Plot showing the dependence of the (RMS) roughness on the time of reduction at -0.8 V vs. Ag/AgCl (KCl_{sat}). (C) Plot showing the dependence of the exponential factor (α) of the constant-phase element, as obtained from EIS, on the (RMS) roughness